Investigation of upper airway changes in orthognathic surgery with computational fluid dynamics analysis

Article *in* Progress in Computational Fluid Dynamics An International Journal · January 2023

DOI: 10.1504/PCFD.2023.10054095

CITATIONS
0

READS
28

6 authors, including:

Frantzeska Karkazi
Marmara University
21 PUBLICATIONS **61** CITATIONS
SEE PROFILE

Erman Aslan
Kocaeli University
30 PUBLICATIONS **40** CITATIONS
SEE PROFILE

Investigation of upper airway changes in orthognathic surgery with computational fluid dynamics analysis

Ilker Inan*

Department of Aircraft Maintenance and Repair,
Istanbul Gelisim University,
TR-34310, Istanbul, Turkey
Email: iinan@gelisim.edu.tr
*Corresponding author

Erman Aslan

Department of Mechanical Engineering,
Kocaeli University,
TR-41380, Kocaeli, Turkey
Email: erman.aslan@kocaeli.edu.tr

Frantzeska Karkazi and Yasemin Bahar Acar

Department of Orthodontics,
Marmara University,
TR-34854, Istanbul, Turkey
Email: fkarkazi@yahoo.com
Email: yacar@marmara.edu.tr

Banu Korbahti and Hasan Riza Guven

Department of Mechanical Engineering,
İstanbul University-Cerrahpaşa,
TR-34320, Istanbul, Turkey
Email: korbahti@iuc.edu.tr
Email: hrguven@istanbul.edu.tr

Abstract: In this retrospective study, computational fluid dynamics (CFD) simulation was used to observe changes in airway in a patient (20-year-old male) who underwent bimaxillary surgery with maxillary advancement and mandibular setback. Bimaxillary orthognathic surgery is an invasive approach that is used for the correction of skeletal class III malocclusion related with dental surgery. In order to perform CFD analysis, at the first stage cone-beam computed tomography (CBCT) data from preoperative (2 months before surgery) and postoperative (6 months after surgery) were used to build the numerical domain at three different volumetric flow rates of 30 L/min, 15 L/min and 7.5 L/min. In addition to volume changes in the airway, pressure drop, shear stress, streamlines were analysed for inhalation and exhalation phases at different volumetric flow rates. The total upper airway volume after the operation narrowed by 13.69% compared to the pre-operation. Upper respiratory tract nasal resistance decreased. In the post-operative condition, a pressure drop was observed between the nostrils and hypopharynx region for all volumetric flow rates. This demonstrates that the patient breathes easier after the bimaxillary orthognathic surgery operation.

Keywords: finite volume method; FVM; turbulent flow; upper airway change; upper airway flow.

Reference to this paper should be made as follows: Inan, I., Aslan, E., Karkazi, F., Acar, Y.B., Korbahti, B. and Guven, H.R. (2024) 'Investigation of upper airway changes in orthognathic surgery with computational fluid dynamics analysis', *Progress in Computational Fluid Dynamics*, Vol. 24, No. 2, pp.100–111.

Biographical notes: Ilker Inan received his BSc in Mechanical Engineering from the University of Sakarya, Turkey, MSc in Energy Systems Engineering from the Gebze Institute of Technology, Kocaeli, Turkey, and PhD in Mechanical Engineering from the İstanbul

University-Cerrahpaşa, İstanbul, Turkey. He is an Assistant Professor of Aircraft Maintenance and Repair Department at Istanbul Gelisim University, Turkey. His main research area is computational fluid dynamics, fluid mechanics and aerodynamics.

Erman Aslan received his BSc, MSc, and PhD in Mechanical Engineering from the University of Sakarya, Turkey. He was a visiting researcher to prepare his PhD thesis at Duesseldorf University of Applied Sciences, Germany. He is an Associate Professor of Mechanical Engineering Department at Kocaeli University, Turkey. His main research area is Lattice Boltzmann method, computational fluid dynamics, forced convection, aerodynamics, and heat transfer.

Frantzeska Karkazi is an MSc student in Orthodontics from the Institute of Health Sciences of Marmara University, Istanbul, Turkey. Her main research areas are clear aligners and digital orthodontics.

Yasemin Bahar Acar received her PhD in Orthodontics from Institute of Health Sciences of Marmara University, Istanbul, Turkey. She is an Associate Professor in Marmara University, Faculty of Dentistry, Department of Orthodontics. Her main research areas are interdisciplinary orthodontic treatments and jaw orthopaedics.

Banu Korbahti received her PhD at Mechanical Engineering Department, Istanbul University, Turkey. She is currently an Associate Professor of Mechanical Engineering Department at İstanbul University-Cerrahpaşa. Her general fields of interest are fluid dynamics and aerodynamics.

Hasan Riza Guven is a retired Professor in Energy Devision of Mechanical Engineering Department at İstanbul University-Cerrahpaşa, Turkey. He received his MSc degree from Bosphorus University and PhD degree from Yıldız Technical University, Istanbul, Turkey. He had been the Head of Mechanical Engineering Department of the İstanbul University-Cerrahpaşa for three years. He is currently working on numerical investigations for convective heat transfer.

1 Introduction

Orthognathic surgery is required for the correction of maxillomandibular skeletal discrepancies that cannot be corrected by orthodontic treatment alone in skeletal class III patients (Samman et al., 1992). Anteroposterior disharmony in the skeletal class III condition can be a result of mandibular excess or maxillary deficiency, or both (Hong et al., 2011). The surgical correction of these conditions can be achieved using either mandibular setback surgery or bimaxillary surgery (Chen et al., 2007). Surgical changes in jaw positions create reorganisation in surrounding tissues i.e., soft palate, tongue, and pharynx.

Many investigations about postoperative airway changes have involved patients undergoing orthognathic surgery, which may cause obstructive sleep apnea (OSA) due to postoperative airway reduction in Class III correction. Chen et al. (2007) compared the effects of mandibular setback and bimaxillary surgery on the airway, and they found that mandibular setback surgery caused long-term changes in the airway. However, bimaxillary surgery was confirmed to not cause significant changes.

Relationship between pressure drop and minimum cross-sectional area in pharyngeal airway before mandibular setback surgery was investigated using computational fluid dynamics (CFD) in order to prevent iatrogenic obstructive sleep apnea (Yajima et al., 2017). The result of this study suggested that surgeons should consider bimaxillary orthognathic surgery instead of mandibular setback surgery to prevent iatrogenic obstructive sleep apnea when correcting a skeletal Class III malocclusion (Yajima et al., 2017). Park et al. (2012) evaluated the volumetric change of the upper airway space in 36 Class III patients who had undergone bimaxillary surgery and analysed the relation between post-surgical stability and airway changes using cone-beam computed tomography (CBCT). Cephalometric evaluation of pharyngeal airway space changes in 45 patients with skeletal class III deformity who received different skeletal repositioning was investigated retrospectively by Pereira-Filho et al. (2011). The subjects were divided into three groups: first group underwent bimaxillary surgery (23 patients), second group underwent maxillary advancement surgery (15 patients), and third group underwent mandibular setback surgery (seven patients). Consequently, maxillary advancement is most suitable surgical movement in relation to airway dimensional gains.

A healthy adult right human nasal cavity was solved numerically to understand flow characteristics with finite element method (FEM) by Keyhani et al. (1995). The steady-state continuity and Navier-Stokes equations were discretised numerically to catch laminar flow patterns in the nasal cavity at quite breathing flow rates (125 ml/s and 200 ml/s). Velocity field that produced by the numerical study was compared with the experimental results, and they observed that numerical results was so close to experimental measurements at various locations in the airway. Experimental and numerical investigation was done to understand flow field in a realistic respiratory model under

three breathing conditions (7.5 L/min, 15 L/min, and 30 L/min) by Phuong and Ito (2015). Particle image velocimetry (PIV) was used to investigate the flow characteristics of the human airway tract. In numerical study, finite volume method (FVM) based commercial code ICEM-CFD was used. They applied four different Reynolds averaged Navier-Stokes (RANS) equations based turbulence models, these are two low Reynolds (Re) number-type k-ε turbulence models, RNG k-ε model and the SST k-ω model. Numerical results were compared with PIV data and concluded that results had a relatively good agreement in the trachea for all cases.

Wei et al. (2017) compared the changes in volume and airflow behaviour of the upper airway by CFD simulation to estimate the influence of anatomical and physiological airway changes due to different head-neck positions (neutral position, extension position: both head and neck extended, sniffing position: head extended, and neck flexed) on mechanical ventilation. Spalart-Almaras model was used to estimate turbulent air flow characteristics. It is observed that sniffing position improves airway patency by increasing airway volume and decreasing airway resistance. Therefore, sniffing position was suggested for optimal choice for mask ventilation. Turbulent flow characteristics inside a realistic model of the upper airway were investigated numerically and experimentally by Tabe et al. (2021). CT scans were used to get 3D printed model and computational model. Three different airflow rates which are 30 L/min (light breathing), 45 L/min (semi-light breathing) and 60 L/min (heavy breathing) were used. Numerical results and experimental results were comparable. The acquired results presented that the maximum pressure drop occurs in the narrowest part of the larynx region. Additionally, the computational results showed that in the trachea region, the secondary flow structures dissipated faster for the flow rate of 60 L/min compared to the lower breathing rates of 30 L/min and 45 L/min.

Mihaescu et al. (2008b) performed numerical investigations on accurate upper airway model in a patient with OSA. Flow simulations were performed within a commercial CFD code Fluent. Highest axial velocity and shear stress were observed at minimum cross-sectional area (retropalatal pharynx). Lowest pressure was observed in here. Wall shear stress on airway walls may affect the progression of OSA severity over time.

Shah et al. (2016) investigated the numerically pharyngeal airflow characteristics on pre-and post-mandibular setback surgery in 29 patients with class III skeletal dysplasia. CBCT images were used to get upper airway geometry. CBCT scans were obtained at three time points which are before surgery, 6 months after surgery and 1 year after surgery. CFD was used to simulate and characterise the pharyngeal airway. After the mandibular setback surgery, pharyngeal airway volume was decreased, and relative mean negative pressure was increased. Therefore, high-risk patients undergoing a large amount of mandibular setback journey should be evaluated for OSA. CFD simulation was applied to observe and understand flow characteristics in airways in a patient who underwent bimaxillary orthognathic surgery by Song et al. (2020). For CFD simulation, they performed CBCT preoperatively, three days postoperatively and seven months postoperatively. Pressure drop and shear stress values were all increased seven months postoperatively. The velopharynx, oropharynx, and epiglottis have narrow cross-sectional areas and have large velocity and pressure gradients. At same locations, large wall shear stress values are observed.

Wadhwa et al. (2021) investigated numerically the pharyngeal airflow characteristics and their relationship with the skeletal movement of the maxilla and mandible after bimaxillary orthognathic surgery in patients with skeletal class III malocclusion. CBCT datas were acquired before surgery, immediately after surgery and at least six months after surgery. The alterations in maxillary and mandibular position, tongue position and hyoid bone position were analysed. A commercial CFD code ANSYS-CFX was used in computations. The total volume of the upper airway including nasal cavity was reduced by 23% immediately after surgery and recovered to 92.2% of the initial volume six months after surgery. Also, pressure drop was decreased in both immediately after surgery and six months after surgery. Estimated air flow characteristics from ANSYS-CFX were correlated to the surgical changes.

CFD analysis is a fast and effective method for determining the properties of flow fields. The aim of this study is to observe and understand the flow characteristics of upper airway for a patient who underwent bimaxillary orthognathic surgery. This research can give an idea about the effect of volume changes in the pharyngeal channel on problems such as OSA.

2 Materials and methods

2.1 Patient selection

Ethical approval was obtained from Istanbul University-Cerrahpaşa Retrospective Clinical Research Ethical Committee (File number: 74555795) on 4th November 2020.

This was a retrospective study and was conducted on a 20-year-old patient who had increased vertical pattern and skeletal Class III malocclusion due to retrognathic maxilla and big mandible. The lateral cephalometric radiography is shown in Figure 1.

Following orthodontic decompensation treatment with fixed appliances, bimaxillary orthognathic surgery was performed. Surgical plan was determined on NemoStudio NX Pro v.10.4.2 (Software Nemotech SL, Madrid, Spain). The surgery procedure consisted of 5 mm maxillary advancement with one-piece Le Fort I maxillary osteotomy (fixated with two 1.5 mm titanium plates on each side with two screws above and two screws below osteotomy line); and 4 mm mandibular set-back with bilateral sagittal split osteotomies (fixated with titanium plates with two screws on each side of osteotomy line). Postoperatively,

intermaxillary fixation with ideal splint and heavy elastics were used for first two weeks. Splint use was ceased after two weeks, and light elastics were continued for four more weeks.

Figure 1 Lateral cephalometric radiography (see online version for colours)

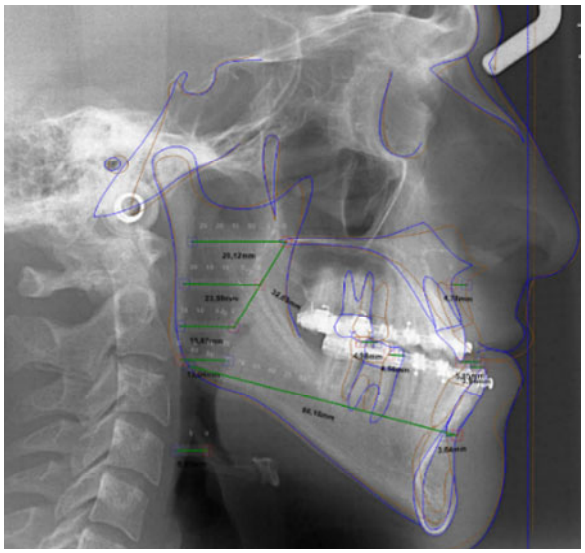

The CBCT data (taken two months before operation (pre-operation) and six months after operation (post-operation) were obtained from Marmara University, Dental Faculty, Orthodontics Department archive. In the next step model reconstruction procedure was performed.

2.2 Model reconstruction

The boundaries of the upper airway and different planes for the cross-sections of the pharyngeal channel are shown in Figure 2. Pharynx consists of hypopharynx, oropharynx, and nasopharynx. Hypopharynx involves epiglottic airway space (EAS), oropharynx contains inferior airway space (IAS), middle airway space (MAS), superoposterior airway space (SPAS) and posterior airway space (PAS). Nasal cavity is located before nasopharynx. It is accepted that the velopharynx part lies between the nasopharynx and oropharynx parts.

CBCT images were used to get numerical airway geometry. A FVM based commercial CFD code ANSYS-Fluent was used in numerical computations. Three different volumetric flow rates which are 30 L/min (heavy breathing), 15 L/min (semi-light breathing) and 7.5 L/min (light breathing) were used (Zhu et al., 2014).

CBCT images were taken at 0.15 mm transverse intervals. CBCT images were used to construct the presented numerical domain. There were two domains, one pre-operation and one post-operation domain. These images were converted into three-dimensional computer models using a medical image processing software Mimics 10.0 (Materialise NV, Leuven, Belgium). To acquire flow domain, the minimum threshold values were used, and radiolucent areas were filled manually. Finally, a three-dimensional flow domain (Figure 3) was created with a computer aided design (CAD) program for:

a pre-operation

b post operation.

Figure 2 The boundaries of the upper airway and different planes for the cross-sectional measurement (see online version for colours)

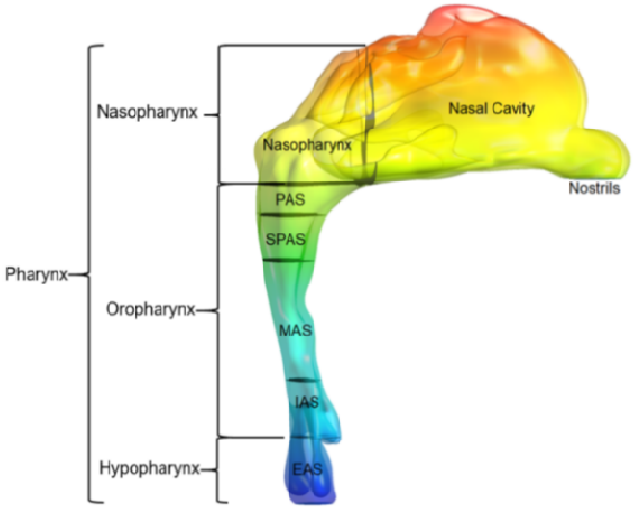

Figure 3 The three-dimensional flow domain created with the CAD program for this study and for (a) pre-operation and (b) post operation (see online version for colours)

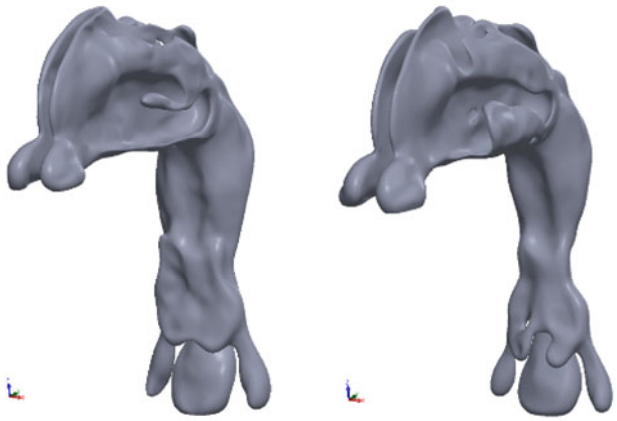

(a) (b)

2.3 Problem definition

Three-dimensional flow domain for pre-operation and post-operation is shown in Figure 3. Expiration and inspiration (respiration) were considered. According to 3D model, positive velocity (from pharynx to nostril) inlet at pharynx and exit from nostril was defined for expiration; while negative velocity (from nostril to pharynx) inlet at pharynx and exit from nostril was defined for inspiration. For representing different respiration simulations, three different air volumetric flow rates were applied: 30 L/min (heavy activity), 15 L/min (light activity) and 7.5 L/min

(calm breathing). The air was maintained at 25°C and atmospheric pressure.

2.4 Mathematical modelling

A FVM-based approach is preferred in the present study, which is based on the commercial, multipurpose CFD code ANSYS Fluent 19.2. The numerical grids were constructed from ANSYS Workbench 19.2. During the numerical simulation, the airflow was assumed to be incompressible and Newtonian. The steady-state assumption was used. Since the respiratory function is a sinusoidal wave cycle, the peak point of this waveform is taken as a flow rate, for modelling expiration and inspiration. The surface of whole upper airway was assumed to be rigid walls. The places of boundary conditions for pre-operation domain are shown in Figure 4. The same boundary conditions were applied at the same places for post-operation.

The expiration and inspiration phases are modelled by changing the inlet boundary condition accordingly. Referring to Figure 4, the boundary condition at the nasal passage is defined to be a pressure boundary, whereas the boundary at pharynx was defined to be a velocity boundary. The expiration is modelled by applying an inflow at the velocity boundary (which implies a positive velocity according to the coordinate system shown in Figure 4), where the flow occurs from pharynx to nostril and an outflow occurs at the pressure boundary. In case of inspiration, an outflow is applied at the velocity boundary (implying a negative velocity according to the used coordinate system), where an inflow is consequently induced at the pressure boundary and the flow direction is from nostril to pharynx. For pre-operation and post-operation, the applied velocities at three flow rates are represented at Table 1.

Table 1 The applied velocities for three flow rates

Volumetric flow rates (L/min)	*Applied velocities for pre-operation process (m/s)*	*Applied velocities for post-operation process (m/s)*
30	4.6172	4.7852
15	2.3086	2.3926
7.5	1.1543	1.1963

In internal flows, velocity can be found in all flow regimes from laminar to fully developed. Although higher order closures are available (Benim, 1990; Xia et al., 1997), a turbulence viscosity model is found to be adequate for present purposes, which can cope with different flow regimes. Therefore, a low Reynolds number k-ω turbulent model was chosen to simulate the airflow in the upper airway tract model, where 'k' indicates the turbulent kinetic energy and 'ω' is the specific dissipation rate. Free shear flow spreading rates in wall-bounded areas can be accurately predicted via this model (Zhang and Kleinstreuer, 2003). In the literature, low Reynolds number k-ω turbulent model was used in numerous investigations (Forman et al., 2007; Inthavong et al., 2010; Liu et al., 2012; Tabe et al., 2021; Paz et al., 2017; Tahavvor and Zarrinchang, 2018) for determining air flow characteristics at the upper airways. ANSYS Fluent (2018) Software was used for solving continuity, momentum (Navier-Stokes), and turbulence model equations. The turbulence intensity and length scale were set to 6% and 0.35 mm, respectively, at the velocity inlet and pressure outlet boundary conditions for pre-operation and post-operation. The turbulent kinetic energy and specific dissipation rate were calculated using the turbulence intensity and turbulent length scale.

Figure 4 Schematic figure of boundary conditions for (a) expiration and (b) inspiration (see online version for colours)

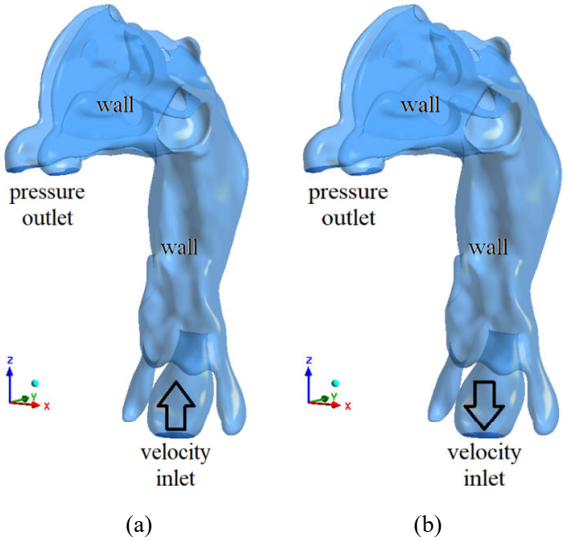

(a) (b)

Figure 5 The constructed grids for (a) pre- operation and (b) post-operation (see online version for colours)

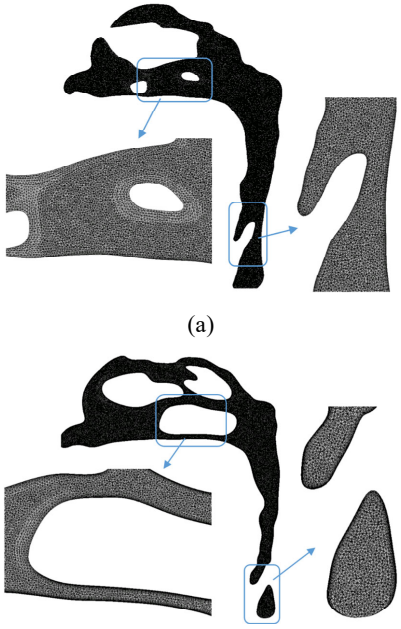

(a)

(b)

Unstructured grid based on tetrahedral elements. The k-ω turbulence model used. Grid resolution was maintained fine for getting y + <2 criteria near the walls. The constructed

grids for pre-operation and post-operation are shown in Figure 5.

2.5 Grid independence study

The grid independency study was performed for pre-operation and post-operation at 30 L/min. The grid independency study was also executed for inspiration and expiration. The resulting grid was then used also for the other lower flow rates. Seven grid densities were applied. The used element size and mesh numbers are listed in Table 2.

Figure 6 The grid independency study pre-operation for inspiration

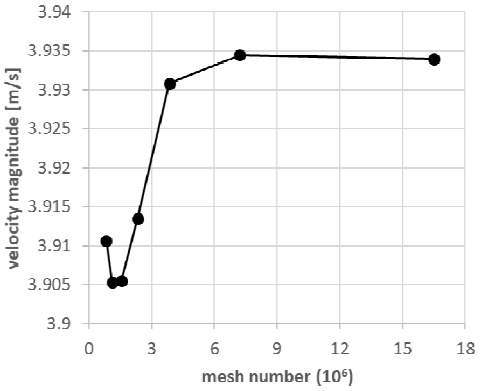

(a)

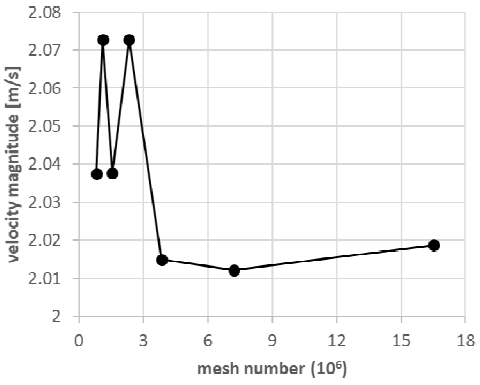

(b)

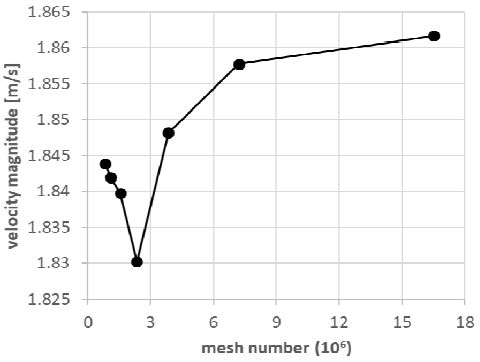

(c)

Figure 7 The grid independency study pre-operation for expiration

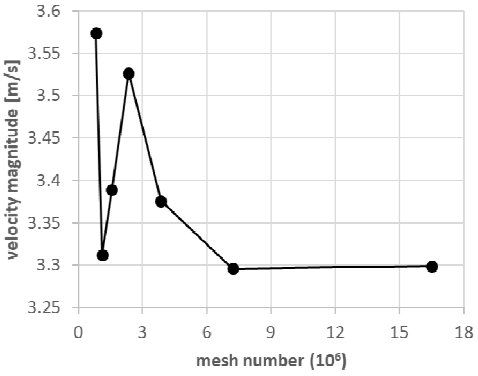

(a)

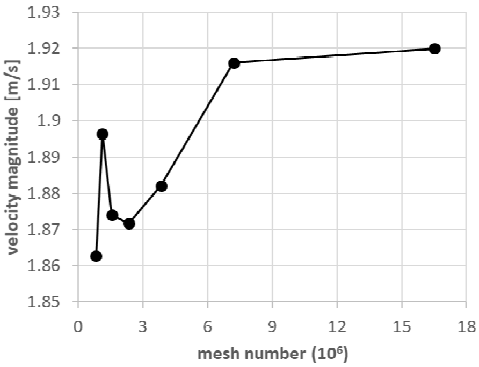

(b)

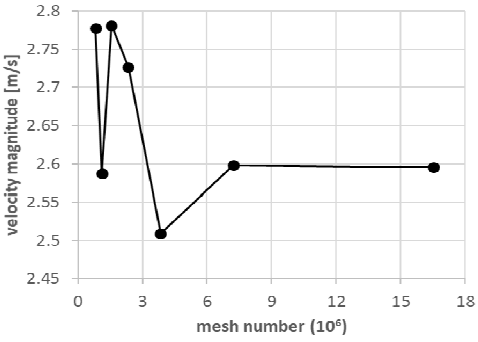

(c)

Table 2 The used element size and mesh numbers

Pre-operation		*Post-operation*	
Element size (mm)	*Total mesh numbers*	*Element size (mm)*	*Total mesh numbers*
0.9	823,369	0.9	754,816
0.8	1,108,056	0.8	999,397
0.7	1,554,477	0.7	1,387,626
0.6	2,335,371	0.6	2,063,729
0.5	3,844,207	0.5	3,368,546
0.4	7,208,299	0.4	6,279,912
0.3	16,509,660	0.3	14,398,054

The velocity magnitude values (m/s) were observed at three sections. These three sections are located at frontal plane, and they are placed 25 mm, 50 mm, and 75 mm away from the nostril. In these sections, area weighted average values are obtained. The grid independency results of pre-operation are shown for inspiration and expiration in Figure 6 and Figure 7, respectively. According to grid independency results of pre-operation, the grid independency mesh numbers are 7,208,299 (0.4 mm element size) for both inspiration and expiration. Additionally, these mesh numbers were used for lower flow rates.

Figure 8 The grid independency study post-operation for inspiration

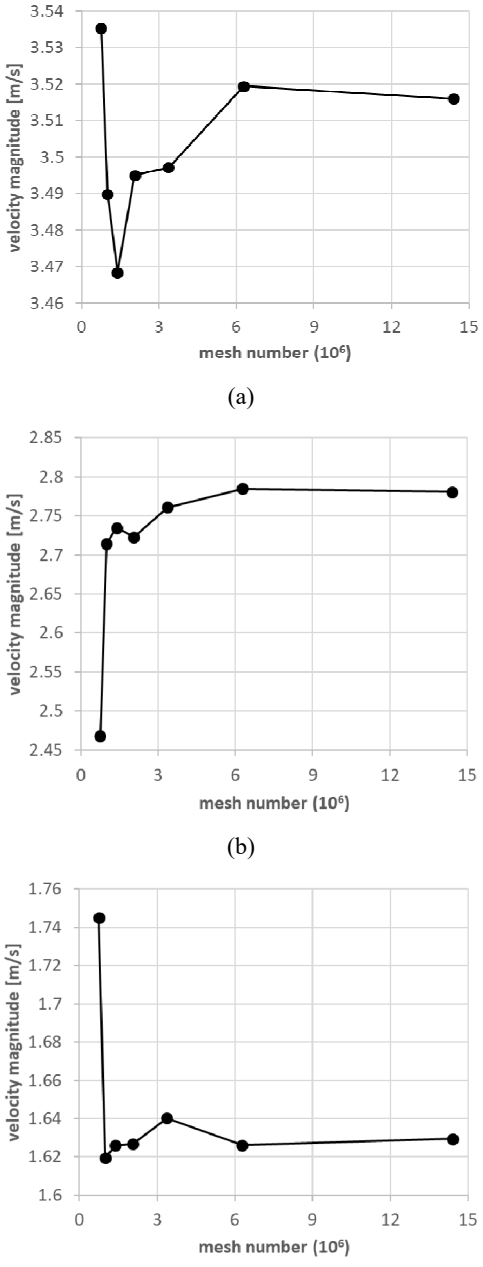

(a)

(b)

(c)

The grid independency results of post-operation are shown for inspiration and expiration in Figure 8 and Figure 9, respectively. According to grid independency results of post-operation, the grid independency mesh numbers are 6,279,912 (0.4 mm element size) for both inspiration and expiration. Additionally, these mesh numbers were used for lower flow rates.

Figure 9 The grid independency study post-operation for expiration

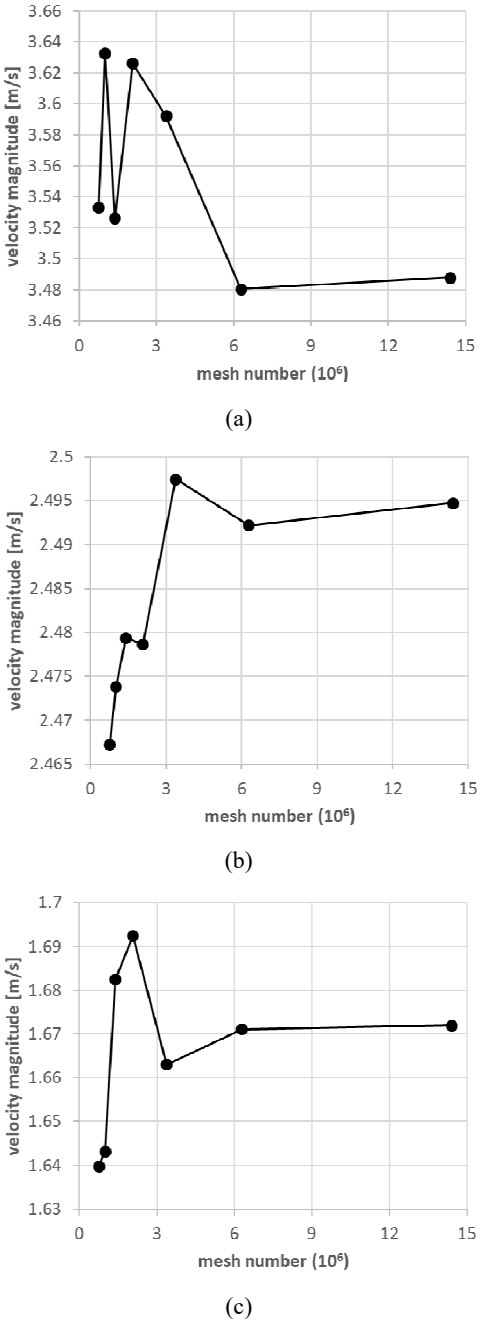

(a)

(b)

(c)

3 Results and discussion

In the light of numerical computations, airway volume changes, flow behaviours (pressure drop, shear stresses, streamlines) were discussed for pre-operation and post-operation, and for different volumetric flow rates, and for expiration and inspiration to make comparisons about

the effect of bimaxillary orthognathic surgery on flow characteristics.

For the pre-operation and post-operation, the total pharyngeal volume and cross sectional area across for different planes in the upper airway were measured from geometrical data. Figure 10 shows the change of volume after operation.

Figure 10 Change in volume after operation

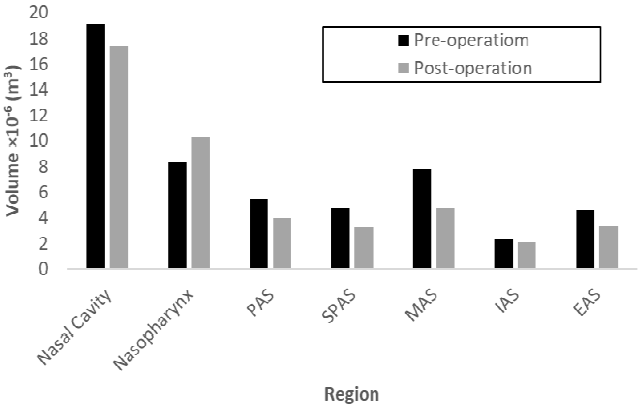

The total upper airway tract volume was 5.25659×10^{-5} m^3 before the operation, the total upper airway tract volume after the operation became 4.53663×10^{-5} m^3. The total volume of the upper airway tract decreased by 13.69% after the operation. Class III correction by bimaxillary orthognathic surgery involves maxillary advancement and mandibular setback. Forward movement of the maxilla acts to increase the upper airway volume; while the backward movement in the mandible acts to reduce the airway volume. In the case of the patient in this study, the backward movement of the mandible (4 mm setback) became more dominant over the volume increase in the maxilla (5 mm advancement), resulting in a reduction of the total upper airway volume. Since post-operation volume increase is not always expected in bimaxillary mandible surgery, narrowing of the upper airway tract after the operation of the patient is one of the expected results.

The static pressure difference (ΔP) was calculated in the region from the nostril to the hypopharynx exit and shown in Figure 11. The investigations in the literature have considered the pressure drop mostly in the region from the nostril to the nasopharynx (Hahn et al., 1993; Riazuddin et al., 2011). Here, the comparisons were generated for inspiration and expiration phases for both pre- and post-operation conditions. In steady state analysis, volumetric flow rates (Q) were considered as 7.5 L/min, 15 L/min and 30 L/min. The flow assumed to be turbulent at all flow rates, and the authors here assume that the turbulence model used in this study can also successfully model laminar conditions.

Pressure drop is higher in pre-operation cases for both inspiration and expiration phases. The inspiration phase creates a higher pressure drop than the expiration phase. The increase in flow rate affects the pressure drop and increasing flow rate increases the pressure drop. Since the nasal resistance (R) is related to pressure drop by:

$$R = \frac{\Delta P}{Q}\left(Pa/L/\min\right) \tag{1}$$

Figure 11 Pressure drop at different volumetric flow rates

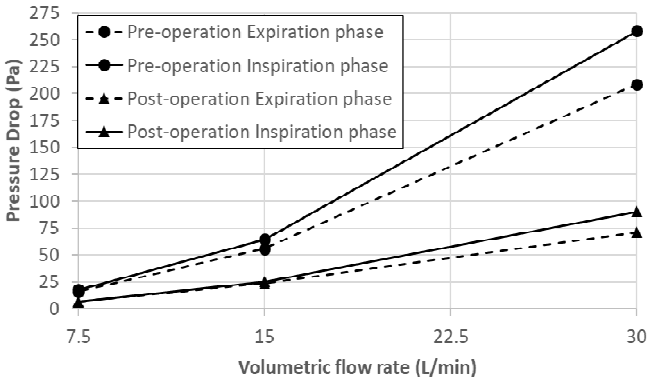

It is obvious that where the pressure drop is high, the nasal resistance will be higher. This means that the nasal resistance in pre-operation case is higher than in post-operation case, according to Figure 11. In the literature, limit values for nasal resistance at certain constant flow rates have been specified for normal individuals (Warren et al., 1992). The nasal resistance values obtained in this study after the operation also seem appropriate when compared with the literature. The nasal resistance during the expiration phase is lower than the inspiration phase for both pre- and post-operation conditions. This result is also compatible with the literature (Riazuddin et al., 2011). At lower flow rates, the pressure drop during inspiration and expiration phases and thus the nasal resistance is remarkably close to each other. The fact that the flow is laminar at low flow rates explains this situation. While the pressure drop for the inspiration and expiration phases start to differ slightly as from 7.5 L/min for the pre-operation condition, it remains constant up to 15 L/min for the inspiration and expiration phases in the post-operation condition. This can be interpreted as the flow, which was predicted to be turbulent at higher flow rates in the pre-operation condition, remaining laminar after operation.

For the upper airway tract modelled within the scope of this study, the wall shear stresses and the streamlines of the upper airway tract system between the nostrils and the hypopharynx are shown in Figure 12 and Figure 13, respectively, for 30 L/min flow rate as contour graphics. In all flow rates, shear stresses during inspiration and expiration phases before the operation were higher than the shear stresses after the operation. The reason for this was the decrease in nasal resistance in the upper airway tract after the operation. Similarly, Ghoneima et al. (2015) told that the upper airway tract resistance decreased after the operation. In the present investigation, the wall shear stresses during expiration phase occurred particularly high in the oropharynx region for all flow rates considered.

Figure 12 Wall shear stress distribution for 30l/min volumetric flow rate (see online version for colours)

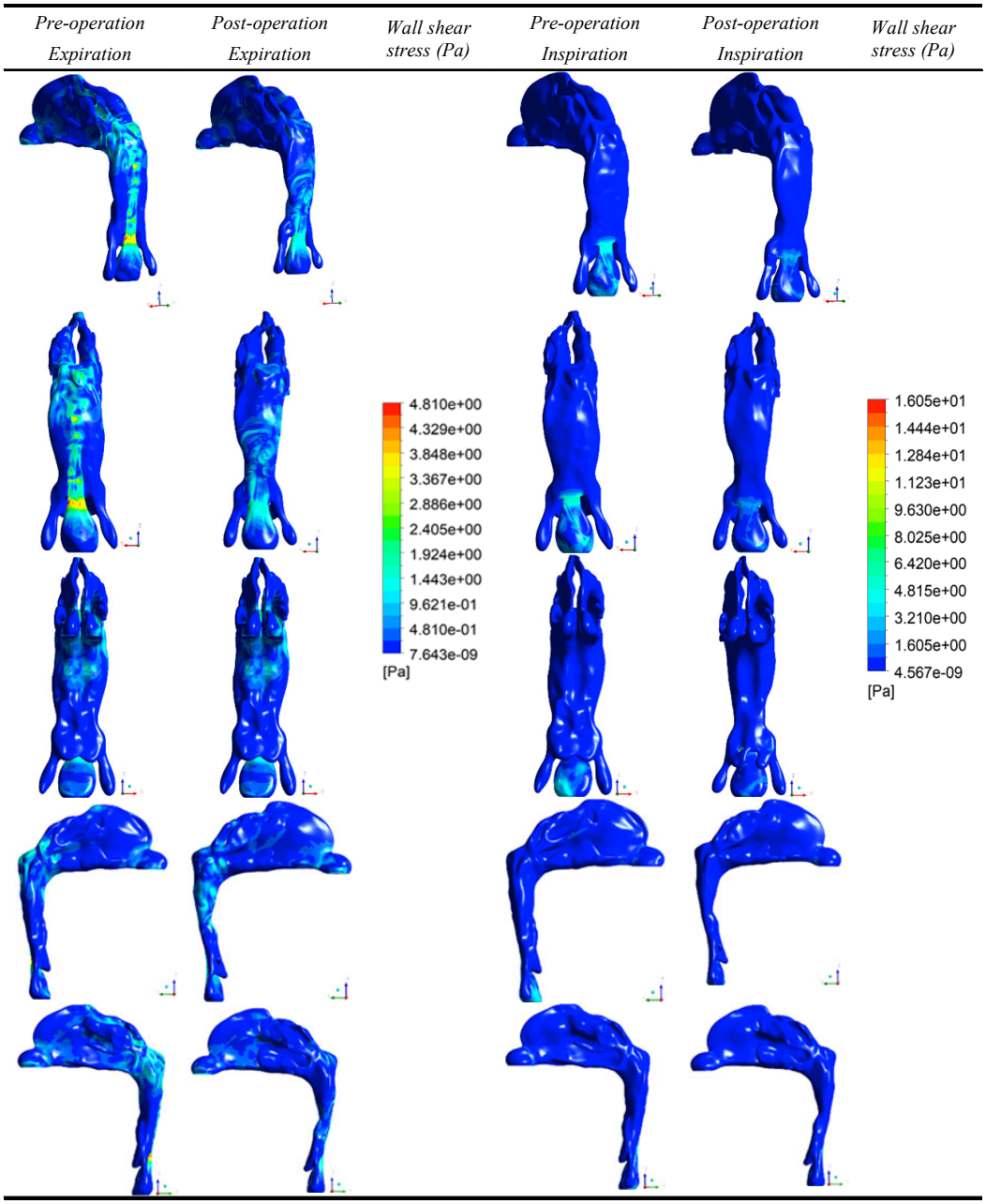

In this region, the wall shear stresses during inspiration were lower than expiration. During inspiration, the region with the highest wall shear stresses was the hypopharynx, and the wall shear stresses during expiration remained lower in this region. This is consistent with the velocity results. Due to individual differences in the anatomical structure of the nasal geometry, it is extremely difficult to draw general conclusions about nasal airflow behaviour. Comparison of results is limited as patient-specific geometries are used. Among the three different flow rates considered, the highest wall shear stresses occurred both before and after the operation at the flow rate of 30 L/min. It is an expected result that the wall shear stresses increase with the increase in the flow rate. Although slightly higher during inspiration, similar flow velocities were obtained in the nasal cavity. However, the flow velocity varied during expiration and inspiration in the pharynx canal for pre- and post-operation. The highest flow velocity during expiration occurs particularly in the oropharynx region. In this region, the flow velocity during inspiration was lower than during expiration. On the other hand, during inspiration, the region with the highest velocity is the hypopharynx, and the velocities during expiration remained lower in this region. This is also consistent with the wall shear stresses. In the pre-operation condition, the flow velocities were always high for both inspiration and expiration phases. The operation has resulted in a decrease in velocities in both phases. During inspiration and expiration, the highest flow velocity both pre- and post-operation occurred at the hypopharynx entrance. The hypopharynx entrance has the smallest cross-sectional area. In addition, this smallest cross-sectional area before the operation was 9.91%

narrower than the area of the same region after the operation. This explains why the flow rate at this point was higher before the operation. Since the Figure 12 and Figure 13 give a qualitative information, which is similar in all three volumetric flow rates, the figures for the other cases was not shown, and it was found sufficient to show the results only for one flow rate.

Riazuddin et al. (2011) claimed that the recirculating flow region was more intense during expiration. However, they examined different regions of the upper airway tract. Presently, expiration phase in the nasopharynx and oropharynx regions also produced more recirculating flow regions than inspiration phase.

Figure 14 shows the variation between expiration and inspiration phases turbulence intensity before and after the operation. The turbulence intensity in expiration phase before and after the operation is higher than inspiration phase. This result is compatible with the literature (Riazuddin et al., 2011). In both inspiration and expiration phases, the pre-operation turbulence intensity is higher than the post-operation turbulence intensity. The turbulence intensity increases as the volume rate increases in inspiration and expiration phases for both pre- and post-operation conditions.

Figure 13 Streamlines for 30 l/min volumetric flow rate (see online version for colours)

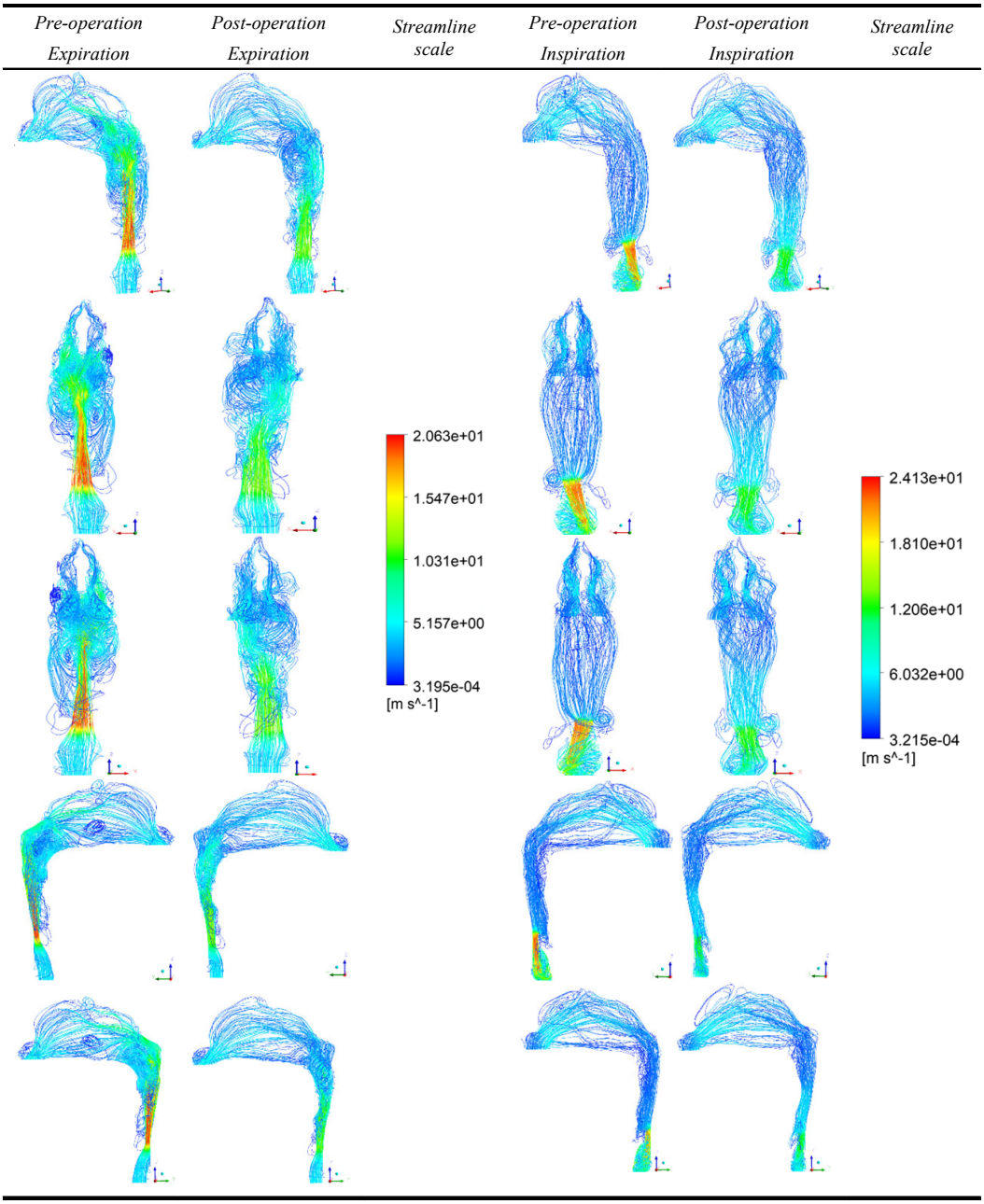

Figure 14 Turbulence intensity variation for pre-and post-operation conditions

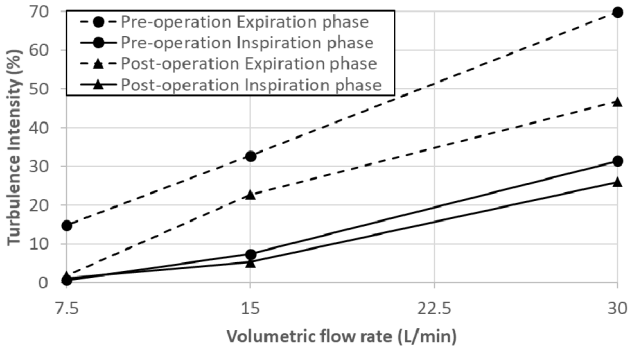

4 Conclusions

The results obtained in this study include the evaluation of the findings obtained from the perspectives of both engineering and dentistry disciplines. The primary aim of this study was to investigate the changes in the upper airway tract flow behaviour between the pre- and post-operation period of a patient who has undergone bimaxillary orthognathic surgery.

The evaluation of volumetric changes within the scope of the study was made according to pre- and post-operation upper airway geometries that were constructed by using CBCT scans taken 2 months before and 6 months after the bimaxillary orthognathic surgery operation of the patient. The total upper airway volume after the operation narrowed by 13.69% compared to the pre-operation. The general idea in the literature on this subject is that the upper airway volume reduction after bimaxillary orthognathic surgery and pressure drop especially in pharynx channel increases the risk of OSA (Wadhwa et al., 2021; Mihaescu et al., 2008a; Wootton et al., 1985). However, although this patient had volume reduction in the PAS, SPAS and MAS regions of the pharynx canal, the patient did not report any complaints about OSA before or after the surgery. It can be thought that this situation is caused by the increase in volume in the nasopharynx region. As a result of this research, it can be concluded that the narrowing of the nasopharyngeal section is more effective in the emergence of the risk of OSA than narrowing of the pharyngeal channel's other sections. Of course, OSA cannot be defined by anatomical factors alone, but the anatomical factor that may be effective for OSA may be the change of volume in the nasopharynx. Because, contrary to the narrowing in all sections after the operation, there has been an enlargement in the nasopharynx section and the patient does not show any OSA symptoms. However, before the operation, the patient did not have any signs of OSA. Thus, it could be possible that the cross-sectional area of the nasopharyngeal part of the channel was sufficient not to cause OSA before the operation. Given this, the current research may help to restrict the question of how much narrowing of the pharyngeal channel can cause OSA, to the question of how much narrowing of the nasopharyngeal section can cause OSA.

The degree of sleep apnea can be judged by the apnea-hypopnea index (AHI). However, in the studies in the literature, exact correlation was not found between AHI and numerical analysis parameters such as wall shear stress, pressure drop and velocity (Taherian et al., 2019). Taherian et al. (2019) tried to find a correlation between the pressure coefficient and the AHI index in their study and concluded that the pressure coefficient gives more reliable correlation than the other factors.

As the flow rate decreases, the pressure drop decreases between the pre- and post-operation during inspiration and expiration phases. Accordingly, the nasal resistance in the upper respiratory tract decreases. At the same time, the pressure drop between the nostrils and hypopharynx region of the upper respiratory tract after the operation is lower than pre-operation condition for all flow rates. This shows that the patient breathes more easily after the operation.

In all flow rates, pre-operation wall shear stresses during inspiration and expiration are higher than post-operation. It was thought that this situation was caused by the decrease in nasal resistance in the upper respiratory tract after surgery. The wall shear stresses during expiration phase occurs particularly high in the oropharynx region. In this region, the wall shear stresses during inspiration are lower than expiration. On the other hand, during inspiration the highest wall shear stresses appeared in hypopharynx region, whereas the wall shear stresses during expiration remained lower in this region. This was consistent with the velocity results. The expiration phase produced more recirculatory flow regions in nasopharynx and oropharynx than the inspiration phase.

The expiration turbulence intensity pre- and post-operation were higher than the inspiration turbulence intensity. The operation caused a decrease in turbulence intensity during inspiration and expiration. Turbulence intensity also decreased with the decrease in flow rate.

Acknowledgements

This research did not receive any funding from funding agencies in the public, commercial, or not for profit sectors.

References

Ansys Fluent (2018) version 19.2, Ansys-Inc., Canonsburg, PA.

Benim, A.C. (1990) 'Finite element analysis of confined turbulent swirling flows', *International Journal for Numerical Method in Fluids*, Vol. 11, No. 6, pp.697–717.

Chen, F., Terada, K., Hua, Y. and Saito, I. (2007) 'Effects of bimaxillary surgery and mandibular setback surgery on pharyngeal airway measurements in patients with Class III skeletal deformities', *American Journal of Orthodontics and Dentofacial Orthopaedics*, Vol. 131, No. 3, pp.372–377.

Forman, M., Jícha, M. and Katolický, J. (2007) 'Aerosol deposition in human airways during breathing cycle', *Applied Computational Mechanics*, Vol. 1, No. 2, pp.437–444.

Ghoneima, A., AlBarakati, S., Jiang, F., Kula, K. and Wasfy, T. (2015) 'Computational fluid dynamics analysis of the upper airway after rapid maxillary expansion: a case report', *Progress in Orthodontics*, Vol. 16, No. 1, pp.1–8.

Hahn, I., Scherer, P.W. and Mozell, M.M. (1993) 'Velocity profiles measured for airflow through a large-scale model of the human nasal cavity', *Journal of Applied Physiology*, Vol. 75, No. 5, pp.2273–2287.

Hong, J.S., Park, Y.H., Kim, Y.J., Hong, S.M. and Oh, K.M. (2011) 'Three-dimensional changes in pharyngeal airway in skeletal class III patients undergoing orthognathic surgery', *Journal of Oral and Maxillofacial Surgery*, Vol. 69, No. 11, pp.401–408.

Inthavong, K., Choi, L.T., Tu, J., Ding, S. and Thien, F. (2010) 'Micron particle deposition in a tracheobronchial airway model under different breathing conditions', *Medical Engineering & Physics*, Vol. 32, No.10, pp.1198–1212.

Keyhani, K., Scherer, P.W. and Mozell, M.M. (1995) 'Numerical simulation of airflow in the human nasal cavity', *Journal of Biomechanical Engineering*, Vol. 117, No. 4, pp.429–441.

Liu, Z., Li, A., Xu, X. and R. Gao (2012) 'Computational fluid dynamics simulation of airflow patterns and particle deposition characteristics in children upper respiratory tracts', *Engineering Applications of Computational Fluid Mechanics*, Vol. 6, No. 4, pp.556–571.

Mihaescu, M., Murugappan, S., Gutmark, E., Donnelly, L.F., Khosla, S. and Kalra, M. (2008a) 'Computational fluid dynamics analysis of upper airway reconstructed from magnetic resonance imaging data', *Annals of Otology, Rhinology & Laryngology*, Vol. 117, No. 4, pp.303–309.

Mihaescu, M., Murugappan, S., Kalra, M., Khosla, S. and Gutmark, E. (2008b) 'Large eddy simulation and Reynolds-averaged Navier-Stokes modeling of flow in a realistic pharyngeal airway model: an investigation of obstructive sleep apnea', *Journal of Biomechanics*, Vol. 41, No.10, pp.2279–2288.

Park, S.B., Kim, Y.I., Son, W.S., Hwang, D.S. and Cho, B.H. (2012) 'Cone-beam computed tomography evaluation of short-and long-term airway change and stability after orthognathic surgery in patients with class III skeletal deformities: bimaxillary surgery and mandibular setback surgery', *International Journal of Oral and Maxillofacial Surgery*, Vol. 41, No. 1, pp.87–93.

Paz, C., Suárez, E., Concheiro, M. and Porteiro, J. (2017) 'CFD Transient simulation of a breathing cycle in an oral-nasal extrathoracic model', *Journal of Applied Fluid Mechanics*, Vol. 10, No. 3, pp.777–784.

Pereira-Filho, V.A., Castro-Silva, L.M., De Moraes, M., Gabrielli, M.F.R., Campos, J.A.D.B. and Juergens, P. (2011) 'Cephalometric evaluation of pharyngeal airway space changes in class III patients undergoing orthognathic surgery', *Journal of Oral and Maxillofacial Surgery*, Vol. 69, No. 11, pp.409–415.

Phuong, N.L. and Ito, K. (2015) 'Investigation of flow pattern in upper human airway including oral and nasal inhalation by PIV and CFD', *Building and Environment*, Vol. 94, No. 2, pp.504–515.

Riazuddin, V.N., Zubair, M., Abdullah, M.Z., Ismail, R., Shuaib, I.L., Hamid, S.A. and Ahmad, K.A. (2011) 'Numerical study of inspiratory and expiratory flow in a human nasal cavity', *Journal of Medical and Biological Engineering*, Vol. 31, No. 3, pp.201–206.

Samman, N., Tong, A.C., Cheung, D.L. and Tideman, H. (1992) 'Analysis of 300 dentofacial deformities in Hong Kong', *The International Journal of Adult Orthodontics and Orthognathic Surgery*, Vol. 7, No. 3, pp.181–185.

Shah, D.H., Kim, K.B., McQuilling, M.W., Movahed, R., Shah, A.H. and Kim, Y.I. (2016) 'Computational fluid dynamics for the assessment of upper airway changes in skeletal class III patients treated with mandibular setback surgery', *The Angle Orthodontist*, Vol. 86, No. 6, pp.976–982.

Song, J.M., Seo, H., Choi, N.R., Yeom, E. and Kim, Y.D. (2020) 'Application of computational fluid dynamics analysis after bimaxillary orthognathic surgery: a case report', *Applied Sciences*, Vol. 10, No. 5, p.1676.

Tabe, R., Rafee, R., Valipour, M.S. and Ahmadi, G. (2021) 'Investigation of airflow at different activity conditions in a realistic model of human upper respiratory tract', *Computer Methods in Biomechanics and Biomedical Engineering*, Vol. 24, No. 2, pp.173–187.

Tahavvor, A.R. and Zarrinchang, P. (2018) 'Numerical simulation of turbulent airflow and micro-particle deposition in upper human respiratory system', *Journal of Applied Fluid Mechanics*, Vol. 11, No. 3, pp.577–584.

Taherian, S., Rahai, H., Lopez, S., Shin, J. and Jafari, B. (2019) 'Evaluation of human obstructive sleep apnea using computational fluid dynamics', *Communications Biology*, Vol. 2, No. 1, pp.1–7.

Wadhwa, P., Jang, H.S., Park, S.H., Kim, H.H. and Lee, E.S. (2021) 'Computational fluid dynamic analysis of the pharyngeal airway after bimaxillary orthognathic surgery in patients with mandibular prognathism', *Processes*, Vol. 9, No. 1, p.152.

Warren, D.W., Walker, J.C., Drake, A.F. and Lutz, R.W. (1992) 'Assessing the effects of odorants on nasal airway size and breathing', *Physiology & Behaviour*, Vol. 51, No. 2, pp.425–430.

Wei, W., Huang, S.W., Chen, L.H., Qi, Y., Qiu, Y.M. and Li, S.T. (2017) 'Airflow behavior changes in upper airway caused by different head and neck positions: comparison by computational fluid dynamics', *Journal of Biomechanics*, Vol. 52, pp.89–94.

Wootton, D.M., Luo, H., Persak, S.C., Sin, S., McDonough, J.M., Isasi, C.R. and Arens, R. (1985) 'Computational fluid dynamics endpoints to characterize obstructive sleep apnea syndrome in children', *Journal of Applied Physiology*, Vol. 116, No. 1, pp.104–112.

Xia, J.L., Smith, B.L., Benim, A.C., Schmidli, J. and Yadigaroglu, G. (1997) 'Effects of inlet and outlet boundary conditions on swirling flows', *Computers & Fluids*, Vol. 26, No. 8, pp.811–823.

Yajima, Y., Oshima, M. Iwai, T., Kitajima, H., Omura, S. and Tohnai, I. (2017) 'Computational fluid dynamics study of the pharyngeal airway space before and after mandibular setback surgery in patients with mandibular prognathism', *International Journal of Oral and Maxillofacial Surgery*, Vol. 46, No. 7, pp.839–844.

Zhang, Z. and Kleinstreuer, C. (2003) 'Low Reynolds number turbulent flows in locally constricted conduits: a comparison study', *AIAA Journal*, Vol. 41, No. 5, pp.831–840.

Zhu, J.H., Lim, K.M., Thong, K.T.M., Wang, D.Y. and Lee, H.P. (2014) 'Assessment of airflow ventilation in human nasal cavity and maxillary sinus before and after targeted sinonasal surgery: a numerical case study', *Respiratory Physiology & Neurobiology*, Vol. 194, pp.29–36.